Liquid Crystals
Publication details, including instructions for authors and subscription information:
http://www.informaworld.com/smpp/title~content=t713926090

Phase behaviour of the discotic mesogen 2,3,6,7,10,11-hexahexylthiotriphenylene (HHTT) under hydrostatic pressure

Yoji Maeda[a]; D. S. Shankar Rao[b]; S. Krishna Prasad[b]; S. Chandrasekhar[b]; Sandeep Kumar[b]
[a] Nanotechnology Research Institute, National Institute of Advanced Industrial Science and Technology, 1-1 Higashi, Tsukuba, Ibaraki 305-8565, Japan, [b] Centre for Liquid Crystal Research, Jalahalli, Bangalore-560 013, India,

Online publication date: 06 August 2010

To cite this Article Maeda, Yoji , Rao, D. S. Shankar , Prasad, S. Krishna , Chandrasekhar, S. and Kumar, Sandeep(2001) 'Phase behaviour of the discotic mesogen 2,3,6,7,10,11-hexahexylthiotriphenylene (HHTT) under hydrostatic pressure', Liquid Crystals, 28: 11, 1679 — 1690
To link to this Article: DOI: 10.1080/02678290110075084
URL: http://dx.doi.org/10.1080/02678290110075084

LIQUID CRYSTALS, 2001, VOL. 28, NO. 11, 1679–1690

Phase behaviour of the discotic mesogen 2,3,6,7,10,11-hexahexylthiotriphenylene (HHTT) under hydrostatic pressure

YOJI MAEDA*

Nanotechnology Research Institute,
National Institute of Advanced Industrial Science and Technology, 1-1 Higashi,
Tsukuba, Ibaraki 305-8565, Japan

D. S. SHANKAR RAO, S. KRISHNA PRASAD, S. CHANDRASEKHAR
and SANDEEP KUMAR

Centre for Liquid Crystal Research, Jalahalli, Bangalore-560 013, India

(*Received 3 March 2001; in final form 8 May 2001; accepted 23 May 2001*)

The phase behaviour of the discotic mesogen 2,3,6,7,10,11-hexahexylthiotriphenylene (HHTT) was investigated under hydrostatic pressures up to 500 MPa using high pressure optical and DTA measurements. The known enantiotropic phase transitions of HHTT, i.e. crystal (Cr)–helical phase (H), H–hexagonal columnar phase (Col_h) and Col_h–isotropic liquid (I) were observed up to 32 MPa. Application of hydrostatic pressures above 32 MPa results in the H and Col_h phases becoming monotropic, depending upon the applied pressure. The H phase was observed as a monotropic phase in the pressure region between 32 and about 180 MPa. Thus, the I $\rightarrow$ Col_h $\rightarrow$ H $\rightarrow$ Cr transition sequence appeared only on cooling under these pressures, while the Cr $\rightarrow$ Col_h $\rightarrow$ I transition occurred on heating. Further increases in pressure above a second limiting value leads to the Col_h phase becoming monotropic. Thus the I $\rightarrow$ Col_h $\rightarrow$ Cr transition sequence appeared on cooling, while the Cr $\rightarrow$ I transition was observed on heating. The T vs. P phase diagram based on the data obtained in the heating mode contains two triple points; one is estimated as 40 MPa, 77.2°C for the Cr–H–Col_h triple point and the other is extrapolated as 285 MPa, 118.3°C for the Cr–Col_h–I triple point. These triple points define the upper limits for the appearance of the stable H and Col_h phases, respectively.

1. Introduction

Discotic liquid crystals are composed of disc-shaped molecules with rigid planar central cores to which are attached 6–8 flexible hydrocarbon chains. They form columnar mesophases which are classified according to the symmetry in the packing of the columns. In the commonly observed hexagonal columnar phase (Col_h), the discs stack one on top of another to form columns and the columns in turn organize to a two-dimensional hexagonal lattice; the order within the columns is liquid-like. In 1984, a transition between such a columnar phase and one containing highly ordered columns was observed in 2,3,6,7,10,11-hexahexylthiotriphenylen e (HHTT) [1]:

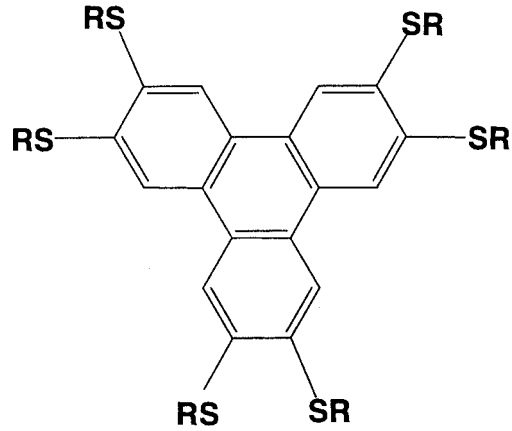

*Author for correspondence; e-mail: yoji.maeda@aist.go.jp

The second phase, which occurs at a lower temperature, has been referred to as the helical (H) phase and

Liquid Crystals ISSN 0267-8292 print/ISSN 1366-5855 online © 2001 Taylor & Francis Ltd
http://www.tandf.co.uk/journals
DOI: 10.1080/02678290110075084

has been seen in only one compound. Detailed X-ray analysis showed that the H phase has the following features: (i) the appearance of (*h k l*) diffraction peaks with non-zero values of *h*, *k*, and *l* indicating that it is a three-dimensionally ordered crystal, which is closely related in structure, however, to the Col_h phase; (ii) the molecules in each column are arranged in a helix with adjacent molecules rotated to minimize the steric energy; (iii) the formation of the H phase is accompanied by the formation of a three-column superlattice. The schematic structures of the H and Col_h phases are shown in figure 1.

The phase transitions of HHTT, Cr–H, H–Col_h, and Col_h–isotropic liquid (I) are observed reversibly at atmospheric pressure. Recently this compound has attracted attention as a functional material having a large photoconductivity, and showing a remarkable hole mobility [2]. Thus, the novel structure [3] and properties of HHTT provided the stimulus for us to investigate the transitional behaviour of HHTT under elevated pressure, and in particular to study the effect of pressure on the stability of the H and Col_h phases. High pressure investigatations of the phase behaviour of liquid crystals helps in the understanding of structure–property relationships for crystal and mesophase polymorphs. Since the first report of pressure-induced mesomorphism [4], many studies on liquid crystals under pressure have been performed [5–15]; however, only a few studies [16–18] have been made concerning the effect of pressure on the mesophases of disc-like molecules. Chandrasekhar *et al.* [16] reported the phase diagram for benzene-hexa-*n*-octanoate (BH8) in which a triple point involving the discotic mesophase was found at about 1.4 kbar. The discotic phase, having a columnar structure with hexagonal symmetry in two dimensions and liquid-like disorder in the third, disappeared at pressures above 1.4 kbar. One of the authors also reported the phase behaviour of the discotic lamellar phase (D_L) of the discotic mesogen 5,10,15,20-tetrakis(4-*n*-dodecylphenyl)-porphyrin (C12TPP). The D_L phase appeared monotropic in the pressure region between 240 and 310 MPa, while the phase was enantiotropic under hydrostatic pressures below 200 MPa [17].

In this paper we report the thermal and optical behaviour of the discotic mesogen HHTT under hydrostatic pressures up to 500 MPa using high pressure optical and differential thermal analysis (DTA) measurements. The effect of pressure on the phase behaviour of HHTT has been studied to elucidate the nature of the mesophase behaviour and also to construct the *T* vs. *P* diagram of HHTT.

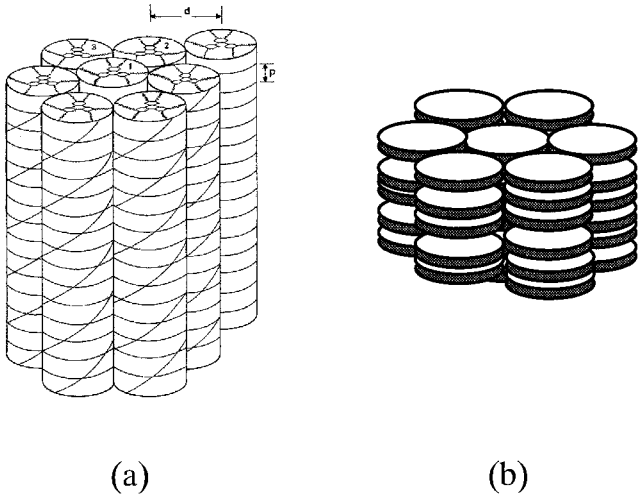

Figure 1. Schematic diagrams of the molecular arrangement in (*a*) the H phase and (*b*) the Col_h phase of HHTT.

2. Experimental

2.1. *Materials*

2,3,6,7,10,11-Hexahexylthiotriphenylen e (HHTT) was prepared using a modification of previously reported methods [1, 19]. Hexanethiol (4.0 g, 17 mmol) was added to a stirred suspension of potassium-*t*-butoxide (2.1 g, 17 mmol) in 1-methyl-2-pyrrolidinon e (20 ml); the solution was heated at 100°C for 10 min and then cooled to 70°C. Hexabromotriphenylene (1.0 g, 1.4 mmol), prepared by the method described by Breslow *et al.* [19], was added and the mixture stirred for 20 min at 70°C. The reaction mixture was poured over ice–water and the product extracted with diethyl ether. The crude product was purified by repeated column chromatography over silica gel (230–400 mesh) eluting with 2–2.5% ethyl acetate in hexane followed by repeated crystallization (four times) from hexane/ether/acetone solution. The final solution was filtered through 0.2 µm filter paper prior to crystallization.

2.2. *Methods*

The high pressure experiments were carried out using optical and DTA systems which are briefly described below.

2.2.1. *Optical apparatus*

The details of the optical high pressure cell have been described in an earlier paper [18]. Essentially it consists of a sample sandwiched between optically polished sapphire rods enclosed in an elastomeric tube. A low viscosity oil was used as the pressurizing medium. At different fixed pressures the intensity of a He-Ne laser beam transmitted through the sample was monitored as a function of temperature using a photodiode with a built-in amplifier, while the sample temperature was varied at a uniform rate of 1°C min^{-1}. The pressure was measured using a precision Heise gauge. A PC handled the data acquisition and control of the experiment.

2.2.2. *DTA apparatus*

The thermal behaviour of HHTT under hydrostatic pressure was studied using a high pressure DTA apparatus described previously elsewhere [20, 21]. The high pressure DTA system was operated in a temperature region between −10 and 250°C under hydrostatic pressures up to 500 MPa. Dimethylsilicone oil (100 cSt, Toshiba Silicone Co.) was used as a pressure transmitting medium. The sample in the DTA cell was coated with epoxy adhesives to fix the material inside the cell and also to prevent the depression of the transition temperatures by the diluent effect of the silicone oil. No diluent effect was observed on comparing the transition temperatures observed in both atmospheric and hydrostatic environments at atmospheric pressure; it was also recognized by inspecting the complete coating of epoxy adhesives after the DTA measurements. Before the DTA runs at each pressure, the sample was heat-treated to 120°C and then cooled to room temperature at 1 MPa. This pretreatment ensured that the DTA measurements had the same starting material and also improved the stability of the DTA baselines having low signal/noise ratios due to the cured epoxy coating. The DTA runs under pressure were performed by heating the sample to the isotropic liquid and then cooling to room temperature. The DTA runs were operated at a constant scanning rate of 5°C min^{-1} under pressure. Transition temperatures were determined as the onset of the transition peak at which the tangent of the inflection point of the peak intersects the extrapolated baseline. Heats of transition were estimated qualitatively by comparison with the heat of melting (28.4 J g^{-1}) of indium under applied pressure, which varies with pressure according to Trouton's rule involving a constant ΔS [22].

3. Results and discussion

3.1. *Phase behaviour*

Figure 2 shows the DSC heating and cooling curves of the HHTT sample at a scanning rate of 5°C min^{-1}. Three distinct endothermic peaks associated with the Cr–H, H–Col_h, and Col_h–I transitions are observed clearly at 64.9°C (31.53 J g^{-1}), 73.5°C (16.33 J g^{-1}) and 93.1°C (9.58 J g^{-1}) on heating, respectively. The Cr–H–Col_h–I phase transitions are observed reversibly under atmospheric pressure. When the sample was cooled rapidly from the isotropic liquid, the helical H phase was observed to quench without crystallization. As a result, a small glass transition of the H glass was found at 12.4°C at a heating rate of 20°C min^{-1}. All of the transition enthalpies are quite large indicating that the transitions have a strong first order character, a feature that is very helpful in DTA experiments. In fact, the Col_h–I transition, which can be considered as a transformation from a two-dimensional solid to a three-dimensional liquid, is the weakest of the three transitions.

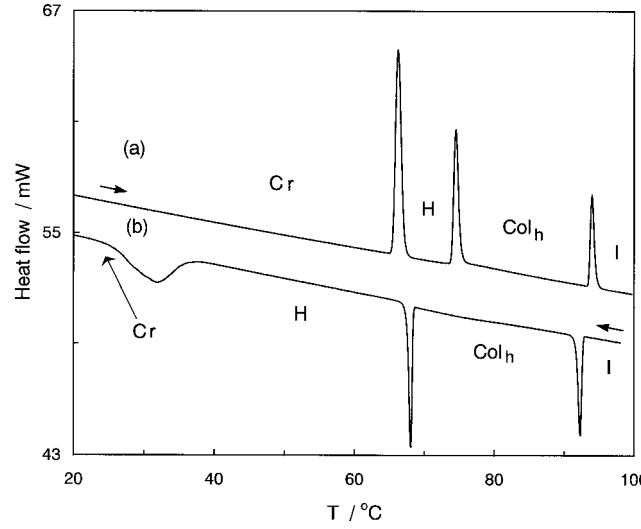

Figure 2. DSC curves obtained with a scanning rate of 5°C min^{-1}. The symbols indicate: Cr crystal, H helical phase, Col_h hexagonal columnar phase, and I isotropic phase.

We summarize here the corresponding structural features of HHTT, observed by X-ray measurements at atmospheric pressure. Figure 3 shows the change in the X-ray patterns obtained on heating the HHTT crystal. The pattern in the H phase exhibits a strong reflection at a spacing corresponding to the intercolumnar distance $d = 21.7$ Å and several wide angle reflections. The latter feature is indicative of the three-dimensional ordering present in this phase. The broad diffuse peak arising from the disordered chains overlaps the sharp peaks associated with the three-dimensional structure of the H phase and therefore is not identifiable, but the sharp peak arising from the core–core distance of about 3.6 Å is very clearly seen. The H phase exists in a relatively narrow temperature region of about 8°C. In the Col_h phase, besides the three low angle peaks whose spacings can be indexed to a 2-dimensional hexagonal lattice, there is a broad diffuse peak corresponding to a mean spacing of 4.7 Å, and a relatively sharp peak arising from a spacing of about 3.6 Å. The former arises from the disordered configuration of the chains and the latter from the well ordered cores. This X-ray pattern reveals the disordered column packing in the Col_h phase. The intensity of the low angle reflection decreased gradually with increasing temperature. It is found that the low angle reflection does not disappear completely at the Col_h–I transition, but remains as an amorphous halo at temperatures above 92°C. This suggests a disordered arrangement of HHTT discs in the molten state just above the Col_h–I transition. The reversible nature of the

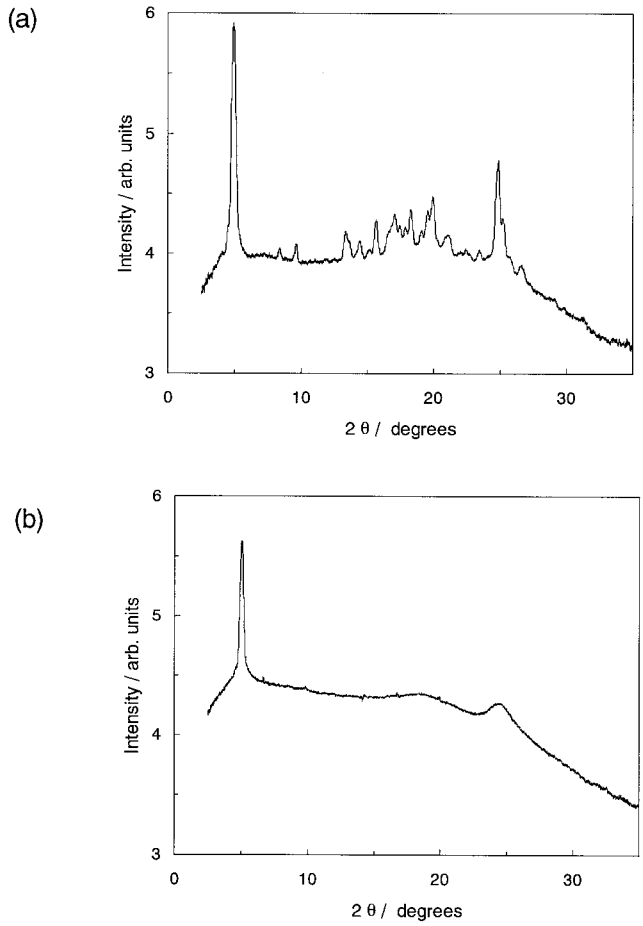

Figure 3. Representative X-ray scans in (*a*) the H phase, depicting the three-dimensional ordering and (*b*) the Col_h phase with fluid-like columns.

$Cr–H–Col_h–I$ transition sequence was shown experimentally by the X-ray diffraction measurements. Thus, the structural phase transitions correspond completely to the thermal behaviour seen using DSC and shown in figure 2.

3.2. *Optical transmission measurements*

Figure 4 (*a*) shows the temperature dependence of the laser transmission through the sample taken during heating under atmospheric pressure. The transitions are identified by abrupt variations in the intensity; the temperatures thus obtained agree well with the values from microscopic and DSC measurements. A particular feature that should be emphasized is that the freezing transition which seldom occurs at a unique temperature (its value usually being determined by a variety of factors such as the rate of cooling, sample history, surface conditions and the presence of nucleation sites), in these experiments, providing the cooling rate was kept constant, did occur repeatedly at the same temperature.

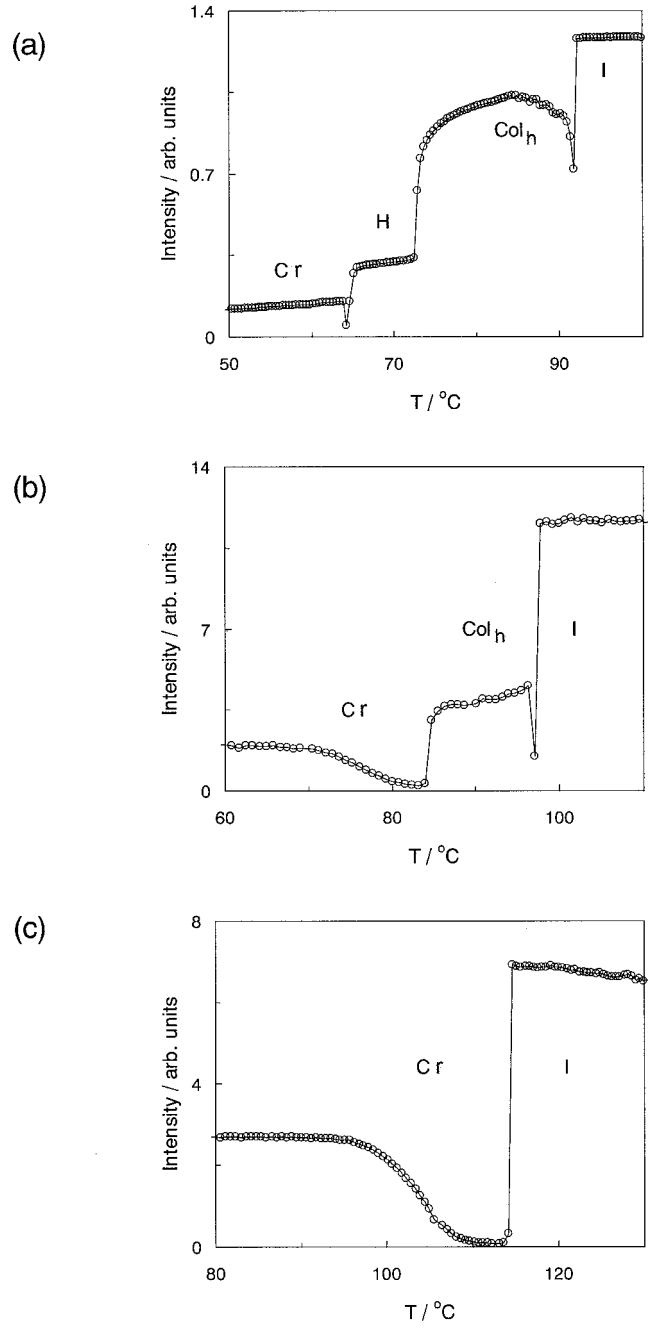

Figure 4. Temperature dependence of the laser transmission recorded during heating (*a*) under atmospheric pressure, (*b*) at a pressure of 80 MPa and (*c*) at 260 MPa.

Another feature, though trivial, which needs to be mentioned is that owing to their first order character, all the transitions exhibited significant thermal hysteresis.

The scans obtained at elevated pressures of 80 and 260 MPa are shown in figures 4 (*b*) and 4 (*c*), and show qualitatively significant differences from the scan at atmospheric pressure. Compared with the three transitions seen at atmospheric pressure, the 80 MPa scan

reveals only two transitions and the one at 260 MPa just one. We identify these changes, tentatively, with modifications of the phase transition sequence as the pressure is increased. The sequence Cr–H–Col_h–I at atmospheric pressure becomes Cr–Col_h–I in the scan at 80 MPa and finally Cr–I in the trace at 260 MPa. In the next section, we substantiate these observations by DTA measurements under hydrostatic pressure.

3.3. *DTA measurements*

3.3.1. *Monotropic transition of the H phase in the low pressure region*

Figures 5 and 6 show the DTA heating and subsequent cooling curves of HHTT under various hydrostatic pressures. The reversible Cr–H–Col_h–I transition behaviour was observed under pressures up to about 30 MPa. The X-ray structural studies under hydrostatic pressure, which will be reported in a forthcoming publication, also support the Cr–H–Col_h–I reversible phase transition sequence under pressures up to 30 MPa. One can see from figure 5 that in the heating process, the Cr–H and H–Col_h transition peaks become closer with increasing pressure and then the two peaks merge into the Cr–Col_h transition peak at about 33 MPa. The H phase could not be observed on heating under pressures above 33 MPa, while the phase can be observed clearly on cooling under pressures up to 180 MPa, as shown in figure 6. Accordingly, the H phase is assigned as a monotropic phase in this pressure region. The thermodynamic metastability of the H phase will be analysed in the next section. In figure 6 one can see that the H → Cr transition (crystallization) peak rapidly shifts to a higher temperature with increasing pressure. Unlike in the optical experiments, it was found that the H → Cr transition was strongly influenced by thermal history on repeated cycling, although the transitions in the heating mode were reproducible. One can see the wide distribution of the Col_h → Cr or H → Cr transition (solidification) points on cooling in the low pressure region below 160 MPa in figure 14. Figures 5 and 6 clearly show the monotropic nature of the H phase under pressures between 33 and about 200 MPa: specifically, the DTA curves at 50 and 125 MPa show the Cr → Col_h → I transition behaviour on heating and also the I → Col_h → H → Cr transition on cooling, respectively.

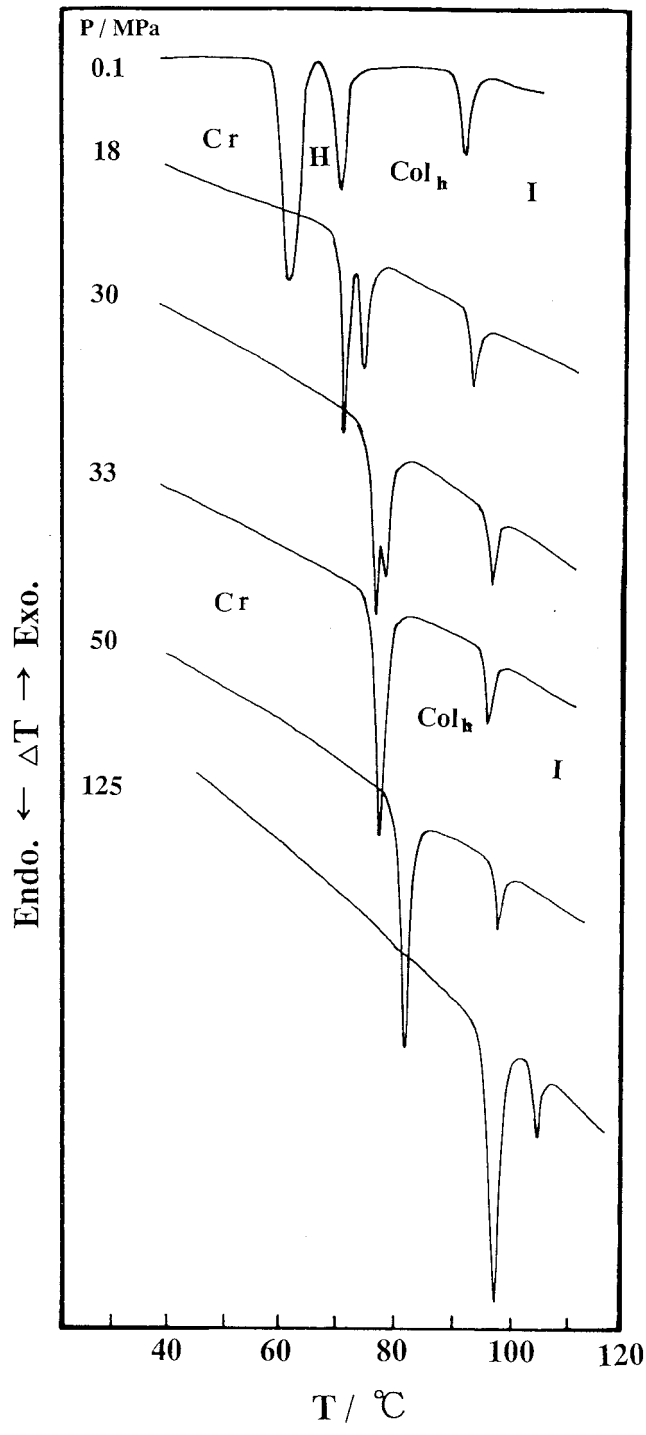

Figure 5. DTA heating curves at various hydrostatic pressures. Heating rate: 5°C min^{-1}.

3.3.2. *Monotropic transition of the Col_h phase in the high pressure region*

As observed in the optical experiments, a further increase in pressure induces a change in transition behaviour of HHTT. Figures 7 and 8 show the DTA heating and subsequent cooling curves of HHTT under various high pressures. The main peak, the Cr → Col_h transition with a shoulder associated with the Col_h → I transition, was observed on heating at 205 and 220 MPa, while these transitions were well separated on cooling. In the heating race, the two peaks come closer with increasing pressure and finally merge into a single peak associated with the Cr–I (melting) transition at pressures

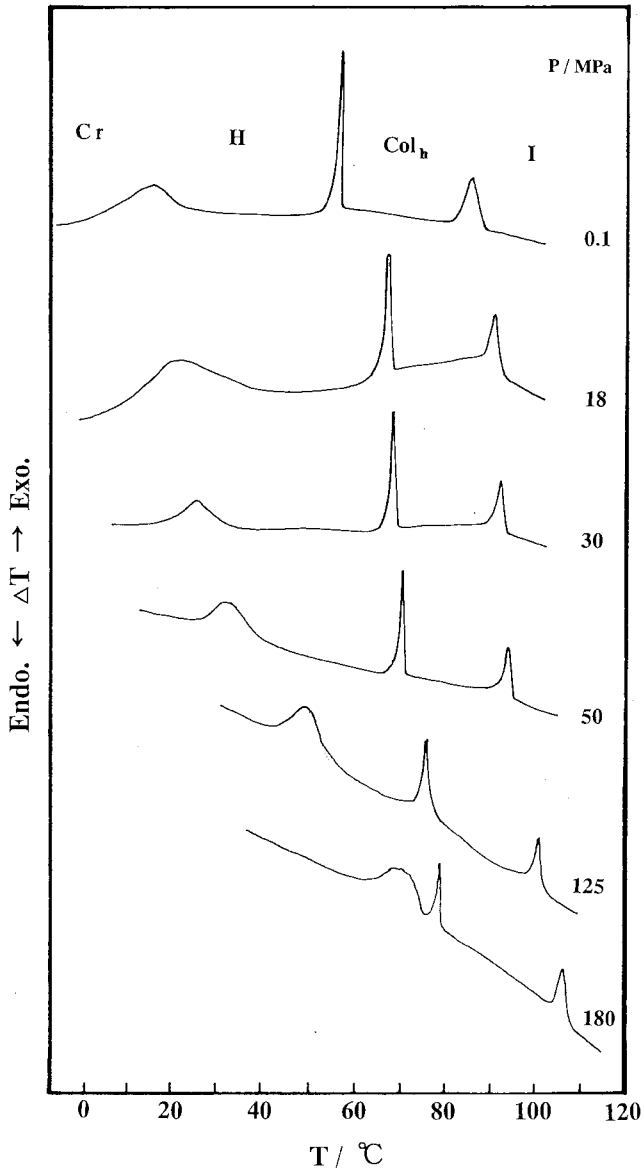

Figure 6. DTA cooling curves at various hydrostatic pressures measured following heating shown in figure 5. Cooling rate: 5°C min^{-1}.

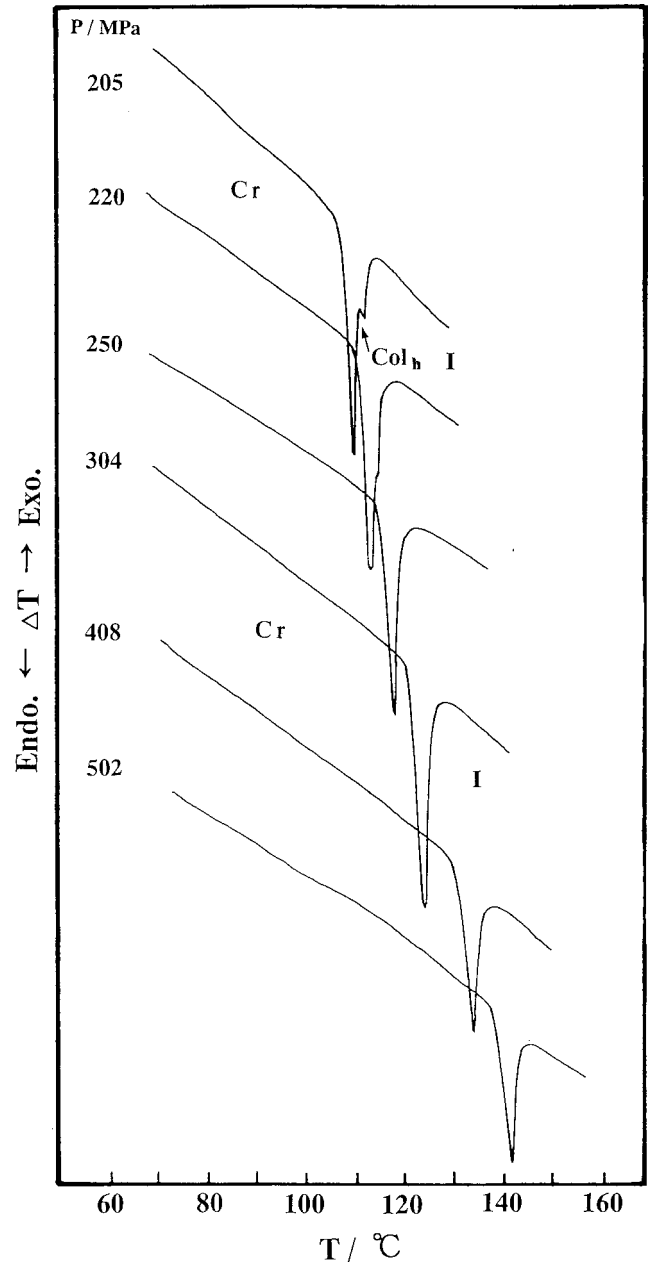

Figure 7. DTA heating curves at high pressures; heating rate 5°C min^{-1}.

above 250 MPa. Hence, only one peak, the Cr–I transition, was observed on heating up to the highest pressure of 502 MPa. In contrast, two peaks, the I–Col_h and $Col_h \rightarrow$Cr transitions, were observed on cooling as shown in figure 8. Accordingly, the Col_h phase can be assigned as a monotropic phase at such high pressures. As shown in figure 8, the $Col_h \rightarrow$Cr transition (crystallization) peak at high pressures shows multiple peaks, suggesting a complex solidification process. The thermal behaviour for the phase stability of the Col_h phase will be analysed in the next section. The X-ray structural studies performed at 250 MPa, confirm the phase sequence and the monotropic nature of the Col_h phase.

3.3.3. *Thermal behaviour of the monotropic phases under pressure*

The H and Col_h phases appear reversibly in the pressure region 0.1–32 MPa and 0.1–220 MPa, respectively. In these pressure regions, the H and Col_h phases behave as thermodynamically stable phases. However, as described in the previous sections, the H and Col_h phases appear only on cooling, i.e. as monotropic phases, in the pressure regions 33–200 MPa and $P > 260$ MPa, respectively. In order to estimate the level of metastability of these phases on the manner of the cooling and subsequent heating

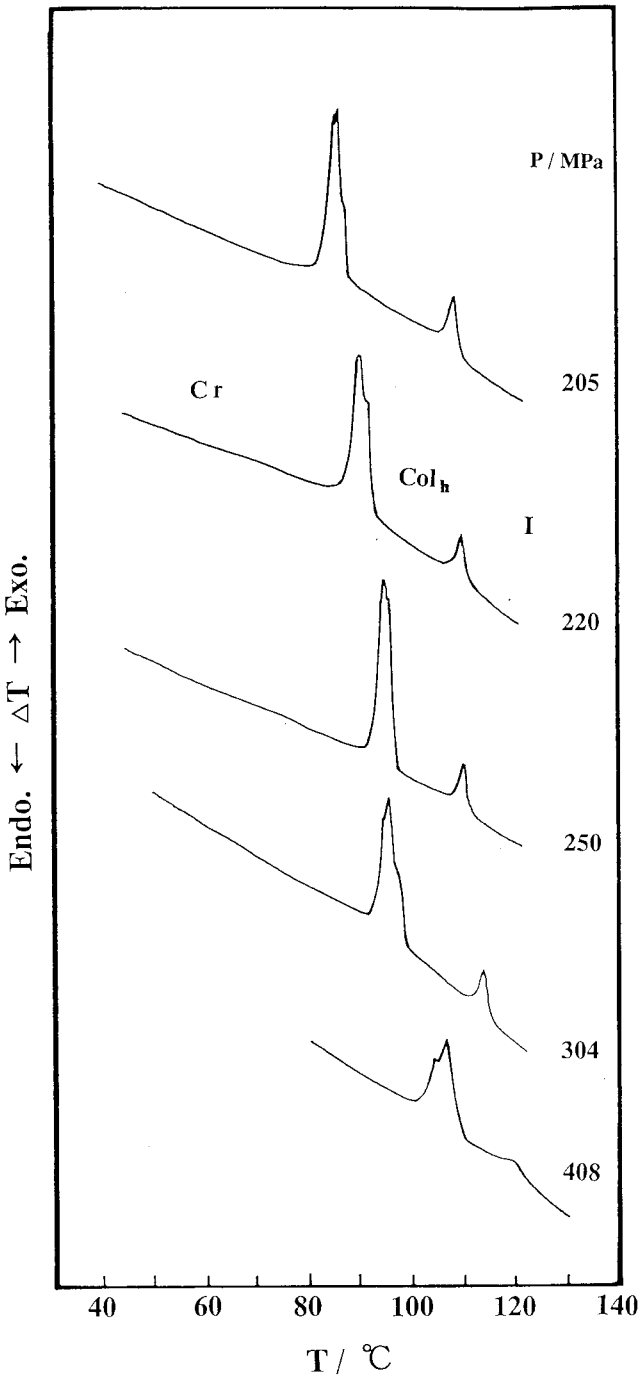

Figure 8. DTA cooling curves of the samples shown in figure 7 at high pressures: cooling rate 5°C min^{-1}.

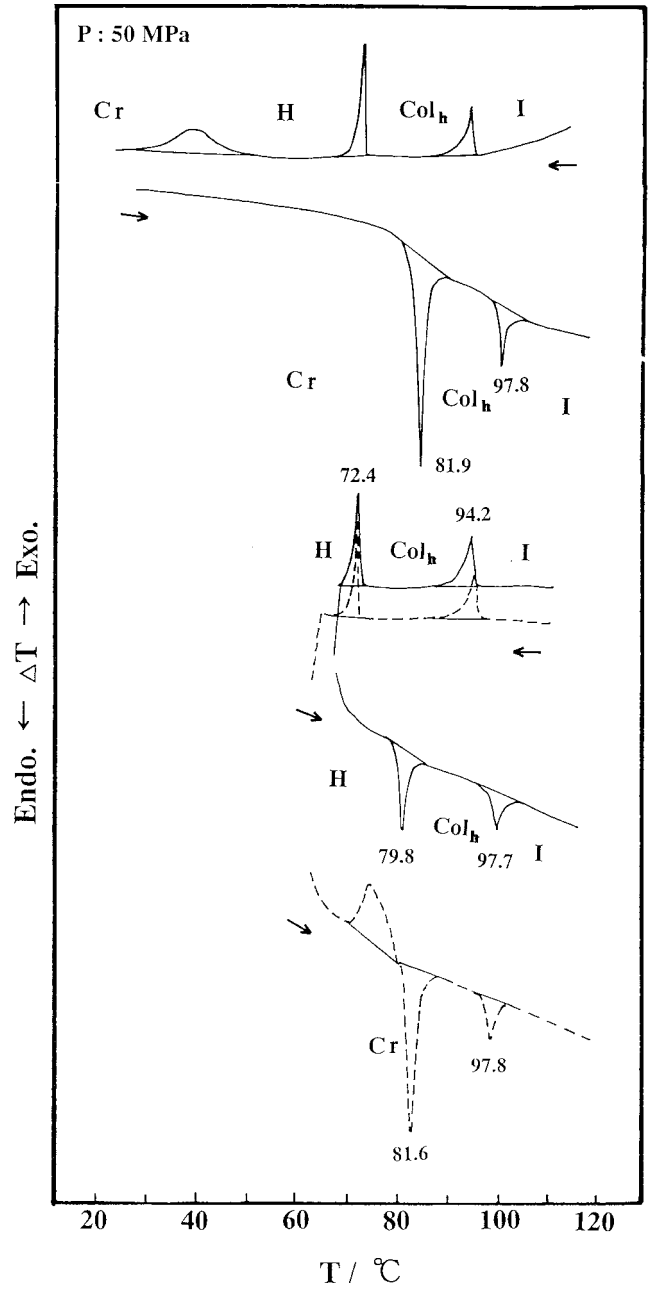

Figure 9. DTA curves of the heat-treated sample at 50 MPa. Temperatures indicated are peak temperatures; scanning rate 5°C min^{-1}.

processes, we performed a series of heat treatment experiments by high pressure DTA under the appropriate pressures. Figure 9 shows the DTA cooling and reheating curves of the heat-treated sample at 50 MPa. The monotropic transitional behaviour of the H phase, i.e. the I → Col_h → H → Cr transition sequence on cooling and the C → Col_h → I transitions on heating at 50 MPa, is observed clearly at this pressure. When cooling was stopped at a temperature in the H phase and the sample immediately reheated into the isotropic phase, a transition peak from the metastable H to the stable Col_h phases was observed at 79.8°C, i.e. 1.8–2.1°C lower than the stable Cr → Col_h transition peak at 81.6–81.9°C. A similar phenomenon was observed at 100 MPa, showing the metastable nature of the H phase more clearly.

On the other hand, the Col_h phase is observed as a thermodynamically stable phase in the pressure region up to 220 MPa. Further increase in pressure results in a change in thermal stability of the Col_h phase. Figure 10 shows the DTA cooling and reheating curves of HHTT at 250 MPa, and reveals the monotropic nature of the Col_h phase, i.e. the $I \rightarrow Col_h \rightarrow Cr$ transition sequence on cooling and $Cr \rightarrow I$ transition on reheating. When cooling was stopped at a temperature in the Col_h phase and the sample reheated to the isotropic phase, a transition from the metastable Col_h to the isotropic phase was observed as a small endothermic peak at 116.3°C, while the stable $Cr \rightarrow I$ transition was observed as a large endothermic peak at 116.7°C. Similar experiments performed at 300 MPa, as shown in figure 11, exhibit the transition from the metastable Col_h phase to the isotropic liquid at a peak temperature of about 118.0°C. On the other hand, the stable $Cr \rightarrow I$ transition was observed with a large endothermic peak at 123.8°C. The difference in the transition temperatures between the metastable Col_h–I and the stable Cr–I transitions reflects the difference in the thermodynamic stability between the Cr and Col_h phases in this pressure range. Such change in thermal stability of the H and Col_h phases under pressure may be illustrated with the help of Gibbs free energy curves as shown in figure 12.

3.3.4. *T vs. P phase diagram of HHTT*

Figures 13 and 14 show the T vs. P phase diagrams of HHTT constructed using both the optical and DTA measurements on heating and cooling, respectively. There is a relatively good agreement between the two data sets based on the optical and DTA measurements, and particularly in the phase diagram for the heating mode. As mentioned earlier, the T vs. P phase diagram for the heating mode is thermodynamically important because it reveals the stable phases. The transition lines obtained by the DTA measurements in figure 13 may be fitted to either first or second order polynomials in pressure as;

0–40 MPa

$Cr \rightarrow H$ transition: $T = 64.4 + 0.436_4 P - 3.35_3 \times 10^{-3} P^2$

$H \rightarrow Col_h$ transition: $T = 72.6 + 0.136_3 P$

40–285 MPa

$Cr \rightarrow Col_h$ transition: $T = 67.3 + 0.257_4 P - 2.93_2 \times 10^{-4} P^2$

0–285 MPa

$Col_h \rightarrow I$ transition: $T = 91.7 + 0.093_6 P$

285–500 MPa

$Cr \rightarrow I$ transition: $T = 88.6 + 0.105_2 P$

The slope of the $Col_h \rightarrow I$ transition line is significantly smaller than those of the $Cr \rightarrow H$ and $Cr \rightarrow Col_h$ transitions and also those of several rod-like liquid crystals [9, 23]. Such a big difference in dT/dP between the $Cr \rightarrow H$ and $Col_h \rightarrow I$ transitions is found in the

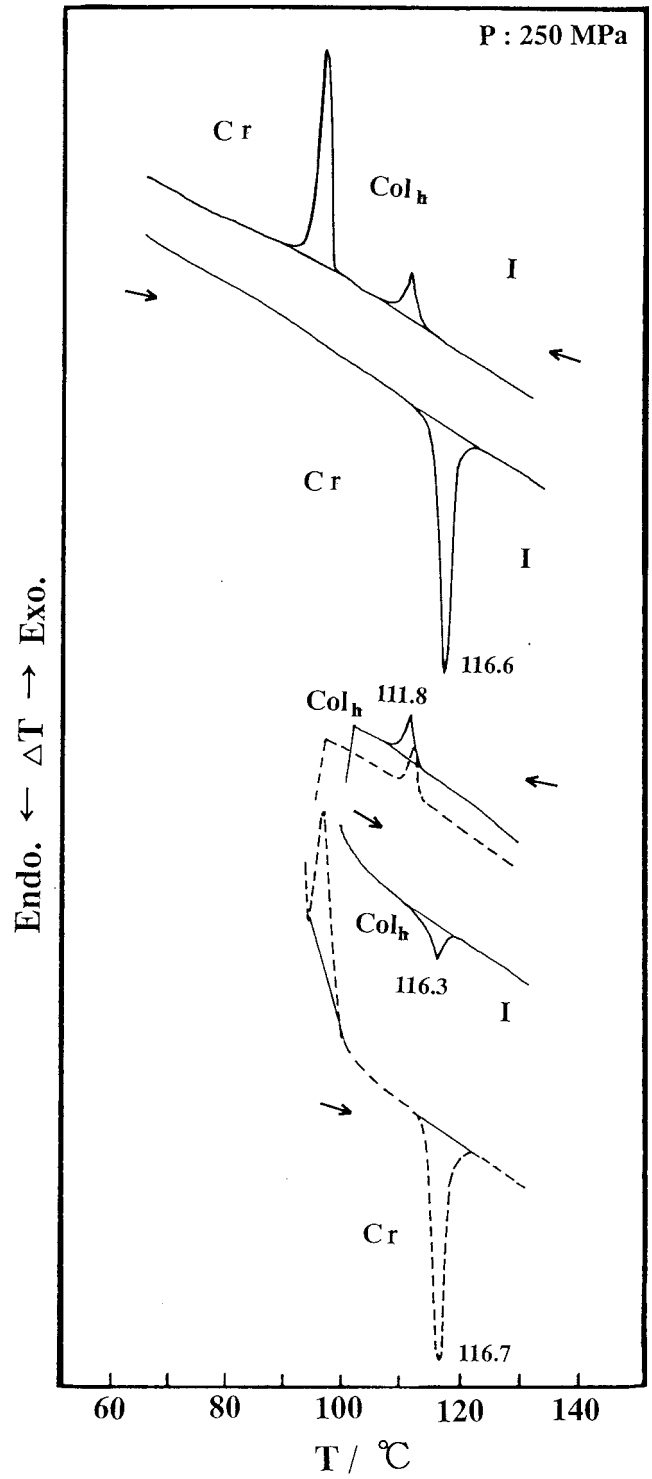

Figure 10. DTA curves of the heat-treated sample at 250 MPa. Peak temperatures are shown in the figure; scanning rate 5°C min^{-1}.

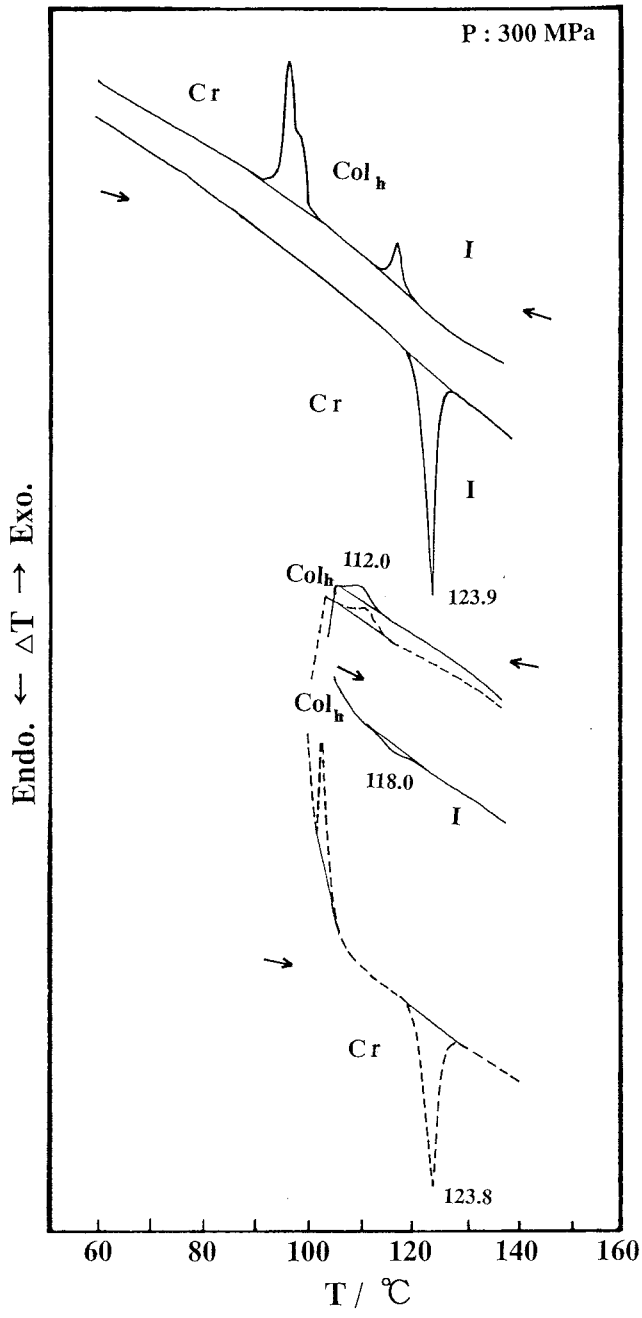

Figure 11. DTA curves of the heat-induced sample at 300 MPa. Temperatures indicated are peak temperatures; scanning rate 5°C min^{-1}.

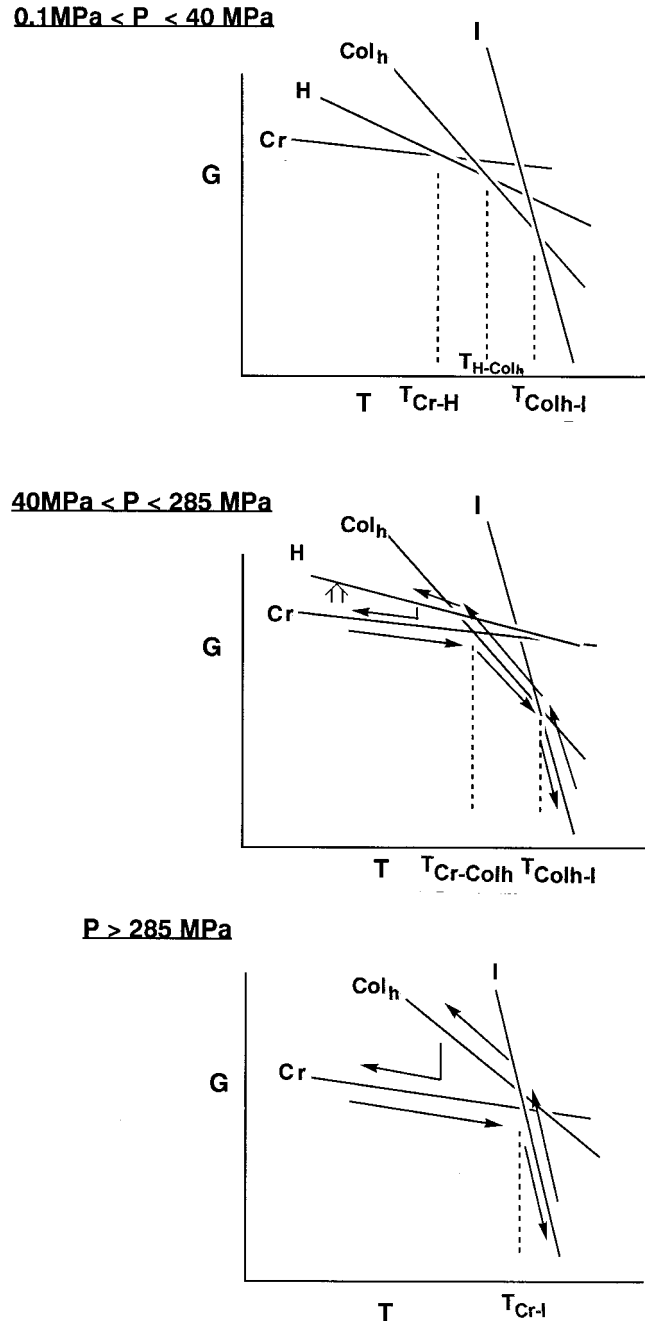

Figure 12. Schematic diagrams of Gibbs free energy vs. T curves.

case of another discotic crystal of 5,10,15,20-tetrakis-(4-*n*-dodecylphenyl)porphyrin: the slope of the $C_5 \rightarrow D_L$ transition is 0.400_1°C MPa^{-1}, while of the $D_L \rightarrow I$ transition is 0.055_3°C MPa^{-1} [17]. It is interesting to note that the Col_h–I transition line takes over smoothly the Cr–I transition with the slope ($dT/dP = 0.105_2$°C MPa^{-1}) at high pressures above 285 MPa.

In figure 13, the temperature range of the H phase decreases with increasing pressure and the H–Col_h transition line meets the melting line at about 40 MPa, thus making the H–Col_h transition monotropic beyond that pressure. Since all the three phase lines, i.e. the Cr–H, H–Col_h, and Cr–Col_h boundaries, are first order in nature, their point of intersection is a simple triple point with the (P–T) coordinates of 40 MPa and 77.2°C, as determined by extrapolating the transition lines to higher pressures. The cooling mode P–T diagram shows thermal destabilization of the H phase with further increases

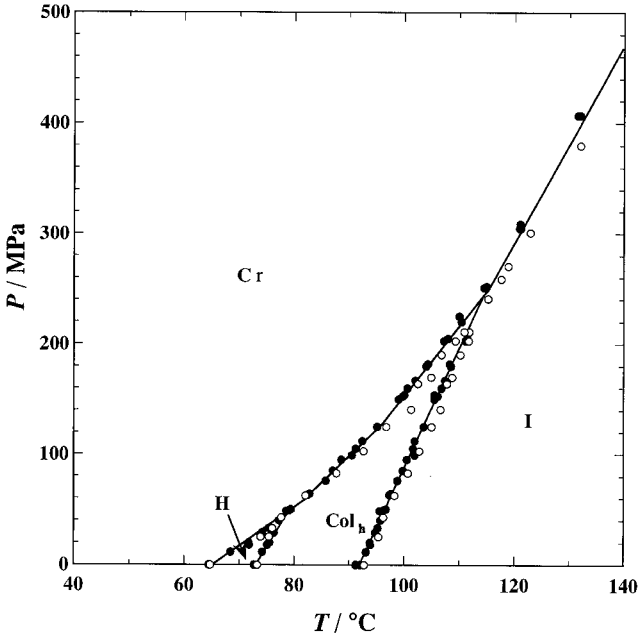

Figure 13. *P* vs. *T* phase diagram for HHTT obtained on heating. Open circles, optical data; filled circles, DTA data.

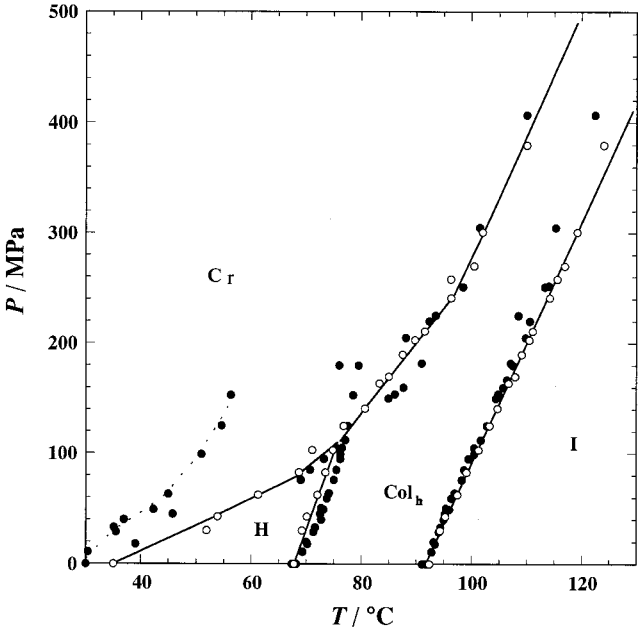

Figure 14. *P* vs. *T* phase diagrams for HHTT obtained on cooling. Open circles, optical data; filled circles, DTA data.

in pressure, and beyond a pressure of ~180 MPa, the H phase does not exist even in the cooling mode.

A similar destabilization of the Col_h phase with increasing pressure is seen in the heating mode. Its temperature range also decreases with increasing pressure, resulting in a second triple point the coordinates of which are 211 MPa, and 111.8°C measured by the optical method, and by extrapolation of the DTA data are 285 MPa, and 118.3°C. Here again, the suppression of the Col_h phase is observed in the heating mode.

These triple points of 40 MPa, 77.2°C and 285 MPa, 118.3°C were estimated by extrapolating the transition lines in figure 13: the former triple point is for the Cr, H, and Col_h phases, and the latter is for the Cr, Col_h, and I phases, indicating the upper limits of the stable H and Col_h phases, respectively. Beyond the second triple point, the Col_h–I transition is monotropic, i.e. observed only on cooling the isotropic phase. However, unlike the case of the H phase, the Col_h phase does not get extinguished in the cooling mode, at least up to the maximum pressure of these measurements. Since the Col_h–I and the crystallization boundaries seem to run parallel to each other, the suppression might not occur even at much higher pressures. It is noted that the metastable regions are strongly influenced by repeated heating and cooling cycles. One can see the wide distribution of the crystallization points ($Col_h \rightarrow Cr$ or $H \rightarrow Cr$ transition points) measured under pressure, as shown in figure 14. These phenomena are probably related to the destabilization of the H and Col_h monotropic phases of HHTT described in the previous sections. Unusual phenomena under pressure are reported also for liquid crystals [24].

The enthalpies of transition of HHTT under pressure were obtained by comparing the standard enthalpy of transition of indium with those of HHTT under hydrostatic pressure. The reproducibility in the transition enthalpy of indium was within ±6%. Combining the slopes (dT/dP) of the transition lines with the transition enthalpies of atmospheric pressure, the volume changes of the transitions at atmospheric pressure were estimated by applying the Clausius–Clapeyron equation, $dT/dP = \Delta V/\Delta S$. The thermodynamic quantities are listed in table 1. It is interesting to see that the ΔV value of the Cr–H transition occupies about 80% of the total ΔV and that the ΔV of the H–Col_h transition is just one fifth of the ΔV of the Cr–H transition. The ΔV value of the Col_h–I transition is only 6% of the total ΔV.

Table 1. Thermodynamic quantities associated with the phase transitions of HHTT at atmospheric pressure.

	Phase transitions		
	$Cr \rightarrow H$	$H \rightarrow Col_h$	$Col_h \rightarrow I$
T/K	338.1	346.6	366.3
ΔH/kJ mol^{-1}	29.3	15.2	8.9
ΔS/J mol^{-1} K^{-1}	86.7	43.8	24.3
dT/dP/K MPa^{-1}	0.351	0.136	0.094
ΔV/cm^3 mol^{-1} [a]	30.4	6.0	2.3

[a] ΔV was estimated by using the Clausius–Clapeyron equation.

Furthermore one can estimate the thermodynamic properties associated with the phase transitions of HHTT using the high pressure DTA data. Table 2 lists the thermodynamic quantities associated with the transitions at 10, 100, and 305 MPa. Unfortunately, the heats of transition under pressure were underestimated by the high pressure DTA measurements. Specifically, the heats of transitions at 10 MPa should approximate to those at atmospheric pressure, see table 1, but the values obtained are about 20% smaller. The main reasons for this difference is the low precision and the low signal to noise ratio of the high pressure DTA apparatus. Nevertheless, it is meaningful to estimate qualitatively the pressure dependence of the volume changes accompanying the transitions of HHTT because the DTA data are self-consistent.

There are a few papers discussing pressure effects on the thermodynamic quantities associated with phase transitions in liquid crystals [9, 23], but just one report involving discotic materials [17]. Thus we attempted to find trends in the thermodynamic quantities of HHTT with pressure. The remarkably small value of the slope dT/dP of the Col_h–I transition ($dT/dP = 0.093_6$°C MPa^{-1}) may be a characteristic feature of columnar discotic liquid crystals. Here it is noted that the Cr–I transition line with the slope $dT/dP = 0.105_2$°C MPa^{-1} takes over smoothly the Col_h–I transition line under high pressures. In table 2, one can see that the dT/dP value decreases dramatically to that of the Cr–I transition under high pressure. The ΔV value is less than 10% of the ΔV of the Cr–H transition because the transition entropy and the slope, dT/dP, of the Col_h–I transition are significantly smaller. On the other hand, the total heats of transitions do not change significantly with pressure. Therefore, it is suggested that for HHTT a significant trend is the decrease in the total ΔV with pressure. Indeed, the ΔV at 300 MPa is about one half that at 10 MPa. In addition, one can see that the value of the transition entropy (20–21 J mol^{-1} K^{-1}) of the Col_h–I transition is approximately constant over the whole pressure range. This supports the relatively higher stability of the Col_h phase of HHTT under pressure.

4. Summary

The transitional behaviour of HHTT changes depending upon the applied hydrostatic pressure. Firstly, the reversible Cr–H–Col_h–I transition sequence can be observed for pressures up to 40 MPa. A further increase of pressure results in a monotropic transition involving the H phase; thus, the metastable H phase is observed only on cooling

Table 2. Thermodynamic quantities associated with the phase transitions of HHTT under hydrostatic pressure.

	Phase transitions at 10 MPa					
	Cr → H	H → Col_h	Col_h → I	I → Col_h	Col_h → H	H → Cr
T/K	341.7	346.8	365.0	363.9	341.3	*c*. 313
ΔH/kJ mol^{-1}	23.0	12.2	7.7	7.1	10.1	—
ΔS/J mol^{-1} K^{-1}	67.3	35.2	21.0	19.5	29.6	—
dT/dP/K MPa^{-1}	0.3507	0.1363	0.0936	0.0806		
ΔV/cm^3 mol^{-1} [a]	23.6	4.8	1.9	1.6		

	Phase transitions at 100 MPa				
	Cr → Col_h	Col_h → I	I → Col_h	Col_h → H	H → Cr
T/K	362.7	372.3	371.6	348.3	327.7
ΔH/kJ mol^{-1}	42.6	7.7	8.0	9.3	28.1
ΔS/J mol^{-1} K^{-1}	117.5	20.7	21.5	26.7	85.7
dT/dP/K MPa^{-1}	0.1833	0.0936	0.0806	0.0667	0.1839
ΔV/cm^3 mol^{-1} [a]	21.5	1.9	1.7	1.8	15.8

	Phase transitions at 305 MPa		
	Cr → I	I → Col_h	Col_h → Cr
T/K	393.4	390.1	369.2
ΔH/kJ mol^{-1}	51.9	6.7	36.9
ΔS/J mol^{-1} K^{-1}	131.9	17.2	99.9
dT/dP/K MPa^{-1}	0.1052	0.0806	0.0966
ΔV/cm^3 mol^{-1} [a]	13.9	1.4	9.6

[a] ΔV was estimated using the Clausius–Clapeyron equation.

in the pressure region between 40 and about 285 MPa. The $Cr \rightarrow Col_h \rightarrow I$ transition sequence is observed on heating, while the $I \rightarrow Col_h \rightarrow H \rightarrow Cr$ transition occurs on cooling in this pressure range. Secondly, a further increase in pressure above a second limiting value induces a monotropic transition involving the Col_h phase; thus, the simple $Cr \rightarrow I$ transition occurs on heating, while the $I \rightarrow Col_h \rightarrow C$ transition sequence appears only on cooling at these higher pressures. The phase transition behaviour of HHTT under pressure can be summarized as,

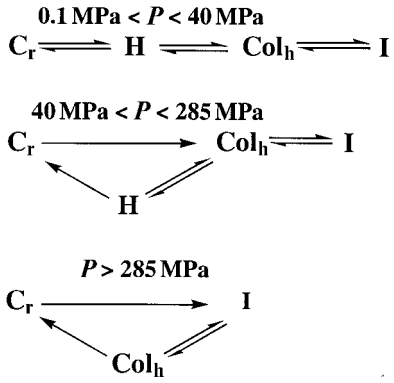

The T vs. P phase diagram constructed from the data obtained in the heating mode clearly exhibits two triple points: one (40 MPa, 77.2°C) is Cr–H–Col_h triple point and the other (285 MPa, 118.3°C) is the Cr–Col_h–I triple point. These triple points define the upper limits of the appearance of the stable H and Col_h phases.

References

[1] Kohne, B., Poules, W., and Praefcke, K., 1984, *Chem. Ztg.*, **108,** 113; Gramsbergen, E. F., Hoving, H. J., de Jeu, W. H., Praefcke, K., and Kohne, B., 1986, *Liq. Cryst.*, **1,** 397.

[2] Adams, J. D., Römhildt, W., and Haarer, D., 1996, *J. appl. Phys.*, **35,** 1826.

[3] Fontes, E., Heiney, P. A., and de Jeu, W. H., 1988, *Phys. Rev. Lett.*, **61,** 1202.

[4] Chandrasekhar,S., Ramaseshan, S., Reshamwala, A. S., Sadashiva, B. K., Shashidhar, R., and Surendranath, V., 1975, *Pramana Suppl.*, **1,** 117.

[5] Keyes, P. H., Weston, H. T., and Daniels, W. B., 1973, *Phys. Rev. Lett.*, **31,** 628.

[6] Feyz, M., and Kuss, E., 1974, *Ber. Bunsenges. phys. Chem.*, **78,** 834.

[7] Spratte, W., and Schneider, G. M., 1977, *Ber. Bunsenges. phys. Chem.*, **80,** 886.

[8] Chandrasekhar, S., 1976, *Rep. Progr. Phys.*, **39,** 613.

[9] Hartmann, M., Jenau, M., Würflinger, A., Godlewska, M., and Urban, S., 1992, *Z. Phys. Chem.*, **177,** 195.

[10] Prasad, S., Khened, S. M., and Chandrasekhar, S., 1993, *Ferroelectrics*, **147,** 351.

[11] Rein, C., and Demus, D., 1993, *Liq. Cryst.*, **15,** 193.

[12] Würflinger, A., 1993, *Int. Rev. phys. Chem.*, **12,** 89.

[13] Shankar Rao, D. S., Krishna Prasad, S., Chandrasekhar, S., Mery, S., and Shashidhar, R., 1997, *Mol. Cryst. liq. Cryst.*, **292,** 301.

[14] Shankar Rao, D. S., Krishna Prasad, S., Veena Prasad, and Sandeep Kumar, 1999, *Phys. Rev. E.*, **319,** 193.

[15] Pollman, P., 1999, in *Physical Properties of Liquid Crystals*, edited by D. Demus, J. Goodby, G. W. Gray, H. W. Spiess and V. Vill (Weinheim: Wiley VCH).

[16] Chandrasekhar, S., Sadashiva, B. K., and Suresh, K. A., 1977, *Pramana*, **9,** 471; Chandrasekhar, S., Sadashiva, B. K., Suresh, K. A., and Madhusudana, N. V., 1979, *J. de Phys. Colloq.*, **C3,** 120.

[17] Maeda, Y., and Shimidzu, Y., 1999, *Liq. Cryst.*, **26,** 1067.

[18] Shankar Rao, D. S., Gupta, V. K., Krishna Prasad, S., Manickam, M., and Kumar, S., 1998, *Mol. Cryst. liq. Cryst.*, **319,** 193.

[19] Breslow, R., Jaun, B., Klutz, R. Q., and Xia, C. Z., 1982, *Tetrahedron,* **38,** 863.

[20] Maeda, Y., and Kanetsuna, H., 1985, *Bull. Res. Inst. Polym. Text.*, **149,** 119.

[21] Maeda, Y., 1990, *Thermochim. Acta*, **163,** 211.

[22] Kutasov, I. M., 1974, *Earth Phys.*, **1,** 75.

[23] Würflinger, A., Sandmann, M., and Weissflog, W., 2000, *Z. Naturforsch.*, **55a,** 823.

[24] Würflinger, A., and Weissflog, W., 2000, *Z. Naturforsch.*, **55a,** 936.